

Effect of different injection strategies considering intravenous injection on combination therapy of magnetic hyperthermia and thermosensitive liposomes

Jiajia Zhu(朱佳佳), Yundong Tang(汤云东), Rodolfo C. C. Flesch(弗莱施 C. C. 鲁道夫), and Tao Jin(金涛)
Citation: Chin. Phys. B, 2024, 33 (**12**): 128703. DOI: 10.1088/1674-1056/ad8a48
Journal homepage: http://cpb.iphy.ac.cn; http://iopscience.iop.org/cpb

What follows is a list of articles you may be interested in

General three-dimensional thermal illusion metamaterials

Tianfeng Liu(刘天丰), Zhaochen Wang(王兆宸), Zhan Zhu(朱展), and Run Hu(胡润)
Chin. Phys. B, 2024, 33 (**4**): 044401. DOI: 10.1088/1674-1056/ad09aa

Extraction method of nanoparticles concentration distribution from magnetic particle image and its application in thermal damage of magnetic hyperthermia

Yundong Tang(汤云东), Ming Chen(陈鸣), Rodolfo C.C. Flesch, and Tao Jin(金涛)
Chin. Phys. B, 2023, 32 (**9**): 094401. DOI: 10.1088/1674-1056/acde50

Enhancement of thermal rectification by asymmetry engineering of thermal conductivity and geometric structure for multi-segment thermal rectifier

Fu-Ye Du(杜甫烨), Wang Zhang(张望), Hui-Qiong Wang(王惠琼), and Jin-Cheng Zheng(郑金成)
Chin. Phys. B, 2023, 32 (**6**): 064402. DOI: 10.1088/1674-1056/acc78c

An optimized smearing scheming for first Brillouin zone sampling and its application on thermal conductivity prediction of graphite

Chengye Li(李承业), Changying Zhao(赵长颖), and Xiaokun Gu(顾骁坤)
Chin. Phys. B, 2023, 32 (**6**): 064401. DOI: 10.1088/1674-1056/ac9223

Experimental investigations of the functional morphology of dragonfly wings

H. Rajabi, A. Darvizeh
Chin. Phys. B, 2013, 22 (**8**): 088702. DOI: 10.1088/1674-1056/22/8/088702

Effect of different injection strategies considering intravenous injection on combination therapy of magnetic hyperthermia and thermosensitive liposomes

Jiajia Zhu(朱佳佳)[1], Yundong Tang(汤云东)[1,†], Rodolfo C. C. Flesch(弗莱施 C. C. 鲁道夫)[2], and Tao Jin(金涛)[3]

[1] *College of Physics and Information Engineering, Fuzhou University, Fuzhou* 350108, *China*
[2] *Departamento de Automação e Sistemas, Universidade Federal de Santa Catarina*, 88040-900 *Florianópolis, SC, Brazil*
[3] *College of Electrical Engineering and Automation, Fuzhou University, Fuzhou* 350108, *China*

(Received 13 August 2024; revised manuscript received 28 September 2024; accepted manuscript online 23 October 2024)

The combination therapy of magnetic hyperthermia and thermosensitive liposomes (TSL) is an emerging and effective cancer treatment method. The heat generation of magnetic nanoparticles (MNPs) due to an external alternating magnetic field can not only directly damage tumor cells, but also serves as a triggering factor for the release of doxorubicin from TSL. The aim of this study is to investigate the effects in the degree of tumor cell damage of two proposed injection strategies that consider intravenous administration. Since both MNPs and TSL enter the tumor region intravenously, this study establishes a biological geometric model based on an experiment-based vascular distribution. Furthermore, this study derives the flow velocity of interstitial fluid after coupling the pressure distribution inside blood vessels and the pressure distribution of interstitial fluid, which then provides the convective velocity for the calculation of subsequent nanoparticle concentration. Different injection strategies for the proposed approach are evaluated by drug delivery result, temperature distribution, and tumor cell damage. Simulation results demonstrate that the proposed delayed injection strategy after optimization can not only result in a wider distribution for MNPs and TSL due to the sufficient diffusion time, but also improves the distribution of the temperature and drug concentration fields for the overall efficacy of combination therapy.

Keywords: magnetic hyperthermia, temperature-sensitive liposomes, intravenous injection, injection strategy

PACS: 87.85.J–, 44.10.+i, 44.05.+e **DOI:** 10.1088/1674-1056/ad8a48

1. Introduction

Magnetic hyperthermia damages malignant cells by the thermogenesis of magnetic nanoparticles (MNPs) after applying an alternating magnetic field.[1–3] On the other hand, thermosensitive liposomes (TSL), as an advanced drug delivery carrier, can release the chemotherapy drug carried internally, doxorubicin (DOX), when their temperature increase to a specific range.[4] Subsequently, DOX can specifically bind to receptors on the surface of tumor cells, which can then be taken up and internalized by tumor cells and ultimately result in drug damage to tumor cells.[5] Because of the heat release characteristics of TSL, the combination of magnetic hyperthermia and TSL can be a good scheme for tumor therapy, in which the heat generated by MNPs in magnetic hyperthermia not only directly damages tumor cells, but also serves as a triggering condition to promote DOX release from TSL. This combination therapy can achieve a dual effect of hyperthermia and chemotherapy, and demonstrate more significant therapeutic effects compared to the use of a single strategy therapy.

In view of the outstanding advantages of combination therapy, many previous studies have begun to conduct in-depth research on various aspects of this combination therapy. Kashkooli *et al*. analyzed the drug delivery and release strategies of nanoparticles in cancer treatment and proposed a scheme of using external stimuli to promote the release of anticancer drugs from nanocarriers, and ultimately confirmed the feasibility of combination therapy.[6] Amin *et al*. conducted a combination therapy experiment of hyperthermia and TSL in mice *in vitro*, described the nanoparticle delivery process in blood vessels, and proposed a two-step mild hyperthermia method.[7] However, this study was limited to *in vivo* treatment in mice and did not consider the actual human situation. Rezaeian *et al*. proposed a drug delivery strategy based on intraperitoneal injection of TSL combined with hyperthermia, which has a better therapeutic effect than traditional chemotherapy, but has a relatively narrow temperature distribution area and also a low drug concentration.[8] Brollo *et al*. combined iron oxide nanoparticles with liposomes to prepare magnetic liposomes, which can release DOX used for therapy when the MNPs temperature increase to a specific threshold under the effect of an external magnetic field.[9] However, this study only discussed the feasibility of magnetic liposomes *in vitro* and did not further investigate the possible issues in actual treatment. Furthermore, Tehrani *et al*. simulated the combination treatment of magnetic hyperthermia and TSL for tumors after establishing a multiscale computational model solved by the finite element method.[10] Although this combination therapy improved the treatment effect and reduced its side effects

[†]Corresponding author. E-mail: tangyundong@fzu.edu.cn

© 2024 Chinese Physical Society and IOP Publishing Ltd

at the same time, the vascular network was not considered in the geometric model of this study and the treatment strategy for this approach was also not optimized.

This study investigates a combination therapy strategy of magnetic hyperthermia and TSL based on a proposed geometric model, in which both MNPs and TSL pass through the blood vessel wall and penetrate into the interstitial region of tumor cells after the intravenous injection.[11] The schematic diagram is shown in Fig. 1(a). In view of the vascular correlation of this approach, this study establishes a relatively complex vascular system based on an experimental image provided in a previous study, and then analyzes the concentration distribution for MNPs after analyzing interstitial fluid velocity, intravascular blood pressure (IBP), and interstitial fluid pressure (IFP). To optimize the effect of treatment, two different injection strategies are proposed in this study, and thermal and drug damages to tumor cells based on concentration and temperature profiles are considered as the evaluation indexes.

2. Methodology

2.1. Proposed geometric model

This study aims to investigate an efficient mechanism of targeted drug delivery by intravenous injection, in which both TSL and MNPs should reach the target tissue by blood circulation within the blood vessels during therapy. For this reason, this paper proposes a simplified geometric model for blood vessel distribution based on an experimental image obtained in vitro in a previous study.[12] As illustrated in Fig. 1(b), the original vascular distribution images can first be converted into grayscale images after removing the invalid characteristics using MATLAB software, and then be created as a hollow blood vessel model by the built-in geometric modeling module of COMSOL Multiphysics software.

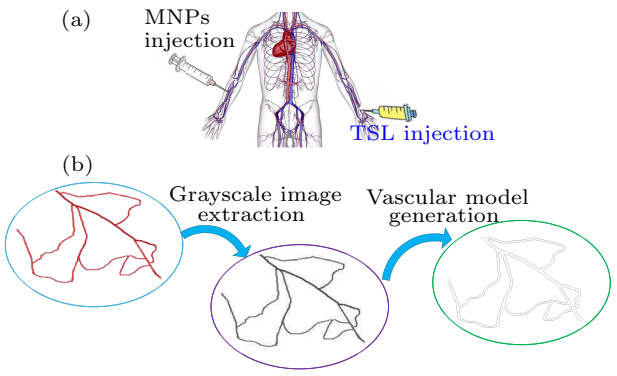


Fig. 1. Overview of the therapy and vascular system representations: (a) schematic diagram of combination therapy, (b) construction process of the geometric vascular model.

Based on this vascular distribution model, this study establishes a biological geometric model used for the intravenous injection behavior, as shown in Fig. 2, which includes the healthy tissue area with a green rectangle, the tumor area with a yellow oval, and the vascular distribution in red, respectively. In addition, this vascular network consists of two inlets and one outlet int the boundaries of the rectangular model.

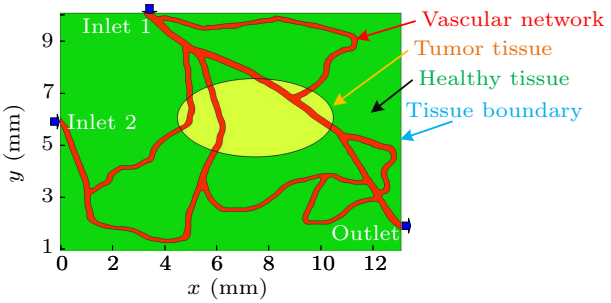


Fig. 2. Proposed biological geometric model.

2.2. Pressure of intravascular blood and interstitial fluid

Both MNPs and TSL reach the malignant tissue through the wall of the blood vessel after intravenous injection. Blood flow is modeled using an incompressible viscous non-Newtonian fluid model during the particle transport,[13] so the fluid flow inside the vascular network can be simulated by the coupling behavior between the Navier–Stokes equation and the continuity equation:[14]

$$\begin{cases} \rho_{\mathrm{b}} \nabla \cdot \boldsymbol{u}_{\mathrm{v}} = 0, \\ \rho_{\mathrm{b}} \left(\boldsymbol{u}_{\mathrm{v}} \cdot \nabla \right) \boldsymbol{u}_{\mathrm{v}} = \nabla \cdot \left[-P_{\mathrm{b}} \boldsymbol{I} + \mu_{\mathrm{b}} (\nabla \boldsymbol{u}_{\mathrm{v}} + (\nabla \boldsymbol{u}_{\mathrm{v}})^{\mathrm{T}}) \right] + \boldsymbol{F}, \end{cases} \tag{1}$$

where the blood parameters ρ_{b}, $\boldsymbol{u}_{\mathrm{v}}$, μ_{b}, P_{b} respectively represent density, flow velocity, viscosity, and pressure. Variable $\boldsymbol{F}$ is the vector of external force acting on a unit volume of fluid.

In addition, the biological tissue can be assumed to be a porous medium, and the interstitial fluid inside biological tissue can also be considered as the Newtonian fluid with incompressible property. Thus, the dynamic equation of interstitial fluid can be obtained after combining the equations of conservation of mass and of momentum[15,16]

$$\nabla \cdot \boldsymbol{v}_{\mathrm{i}} = -\frac{K}{\mu_{\mathrm{i}}} \nabla^2 P_{\mathrm{i}} = \varphi_{\mathrm{b}} - \varphi_{\mathrm{L}}, \tag{2}$$

where $\boldsymbol{v}_{\mathrm{i}}$ and P_{i} indicate the velocity and pressure of interstitial fluid. K and μ_{i} denote separately the penetration rate of porous tissue and the dynamic viscosity of the interstitial fluid. The source term, φ_{b}, represents the fluid flow rate permeating from microvessels into the extracellular matrix, which is also related to blood pressure with the following equation:[17]

$$\varphi_{\mathrm{b}} = L_{\mathrm{p}} \left(\frac{S}{V} \right) \left(P_{\mathrm{b}} - P_{\mathrm{i}} - \sigma_{\mathrm{s}} \left(\pi_{\mathrm{b}} - \pi_{\mathrm{i}} \right) \right), \tag{3}$$

where L_{P}, S, V, P_{b},P_{i}, σ_{s}, π_{b}, π_{i} represent separately the hydraulic conductivity of microvascular walls, the superficial area of blood vessels, and the volume of malignant tissue, the IBP, the IFP, the average osmotic reflectance coefficient of plasma proteome, and the osmolarity of proteome and interstitial fluid. In addition, the sink term, φ_{L}, denotes the fluid rate draining through the lymphatic system as[18]

$$\varphi_{\mathrm{L}} = L_{\mathrm{PL}} \frac{S_{\mathrm{L}}}{V} \left(P_{\mathrm{i}} - P_{\mathrm{L}} \right), \tag{4}$$

where L_{PL}, S_L, P_L denote separately the hydraulic conductivity, the surface area, and the hydrostatic pressure of the lymphatic vessel wall. In addition, the φ_L is zero in malignant tissue due to the absence of an effective lymph system.[19]

2.3. Magnetic fluid concentration and heat transfer

In a porous tissue environment, the movement mechanism of MNPs is driven not only by the diffusion behavior of intermolecular interactions but also by the convection behavior of the interstitial fluid flow. Thus, the concentration distribution of magnetic fluid can be described by the convection diffusion equation as[20]

$$\frac{\partial C_N}{\partial t} = -\nabla\left(v_i C_N\right) + \nabla\left(D_N \nabla C_N\right) + \zeta, \tag{5}$$

where the diffusion coefficient of magnetic fluid, D_N, can be expressed as $D_N = (K_B T/(6\pi a_N \eta))\exp\left[-\left(1+a_N\gamma^2/a_f\right)\right]$. Variables K_B, a_N, η, a_f, γ, C_N represent the Boltzmann constant, MNPs radius, viscosity, the radius and volume fraction of organizational fibers, and concentration of MNPs, respectively. In addition, the source term, ζ, in Eq. (5) can be defined as follows:[21]

$$\begin{aligned}\zeta \;=\; & \varphi_b\left(1-\sigma_N\right)C_{pN} + \lambda\frac{S}{V}\left(C_{pN}-C_N\right)\frac{\delta_N}{e^{\delta_N}-1} \\ & -\varphi_L C_N - \beta C_N.\end{aligned} \tag{6}$$

The symbol δ_N has a further expression as $\delta_N = \varphi_b(1-\sigma_N)/(\lambda S/V)$.[22] Variables σ_N, λ, β denote the osmotic reflectance coefficient of the magnetic fluid, vascular permeability, and drug clearance constant, respectively. In addition, the magnetic fluid concentration in blood vessels, $C_{pN} = C_{0N}\exp(-t/k_{dN})$, has an initial value, C_{0N} =3.5 mol/m^3, before the intravenous injection of magnetic fluid into the human body. The parameter k_{dN} represents the constant decay time of MNPs in the blood.

In the combination therapy of this study, MNPs contained in magnetic fluid will release heat to damage malignant cells when exposed to an external magnetic field after the intravenous injection of MNPs. This heat generation is generally determined by the magnetic fluid concentration and the properties of MNPs and magnetic field, being represented as[23]

$$Q_{MNP} = \theta P_{MNP} = \frac{C_N}{\rho_{MNP}} \cdot \frac{\mu_0^2 M_s^2 V_m H_m^2 f}{K_B T_0} \cdot \frac{2\pi f \tau_{eff}}{1+\left(2\pi f \tau_{eff}\right)^2}, \tag{7}$$

where ρ_{MNP}, μ_0, M_s, H_m, f, τ_{eff}, T, V_m represent MNP density, magnetic conductivity, saturation magnetization, magnetic field strength, magnetic field frequency, effective relaxation time, absolute temperature of MNPs, and volume of MNPs, respectively. Nevertheless, this study does not consider the MNPs material properties for the heat production due to its lower effect on the proposed analysis method.

The power dissipation of MNPs can lead to a rise in the temperature of biological tissue, which can be predicted by the improved Pennes equation, as reported in a previous study[24]

$$\rho_i c_i \frac{\partial T_i}{\partial t} = k_i \nabla^2 T_i + \rho_b c_b \omega_b^i \left(T_b - T_i\right) + Q_m^i + i \cdot \alpha \cdot Q_{MNP}, \tag{8}$$

where different superscript and subscript refer to blood with "b", healthy tissue with "0", malignant tissue with "1", and MNPs with "MNP". Variables ω, ρ, c, k, Q_m represent blood perfusion, density, specific heat volume, thermal conductivity, and biological heat. In order to get closer to the real situation, the blood perfusion rate presented in Eq. (8) can further be described as a temperature-dependent parameter with the following expression:[25]

$$\omega_b^0 = \begin{cases} 4.5\times10^{-4} + 3.55\times10^{-3}\exp\left(\dfrac{-(T-45)^2}{12}\right), & T \le 45\ ^\circ\text{C}, \\ 0.004, & T > 45\ ^\circ\text{C}, \end{cases} \tag{9}$$

$$\omega_b^1 = \begin{cases} 8.33\times10^{-4}, & T < 37\ ^\circ\text{C}, \\ 8.33\times10^{-4} - \dfrac{((T-37)^{4.8})}{5.438\times10^6}, & 37\ ^\circ\text{C} \le T \le 42\ ^\circ\text{C}, \\ 4.16\times10^{-4}, & T > 42\ ^\circ\text{C}. \end{cases} \tag{10}$$

2.4. Drug delivery and druginduced damage

The TSL release rate depends on the difference in temperature distribution, which in turn affects the concentration of the therapeutic drug DOX. TSL moves in the form of nanoparticles in the interstitium, and its concentration dynamics follows the diffusion–convection–reaction equation. The velocity of the interstitial fluid is used as the convective velocity in this case, so the TSL concentration equation can be coupled with Darcy's law and the local temperature value T[26]

$$\frac{\partial C_T}{\partial t} = D_T \nabla^2 C_T - v_i \cdot \nabla C_T - K_{EL} C_T + \psi, \tag{11}$$

where TSL-related parameters C_T, D_T, K_{EL} represent concentration, diffusion coefficient, and drug release rate, respectively. The source term ψ can be expressed in a similar manner to the source term used for the MNPs as[26]

$$\psi = \varphi_b\left(1-\sigma_T\right)C_{PT} + \lambda\frac{S}{V}\left(C_{PT}-C_T\right)\frac{\delta_T}{e^{\delta_T}-1} - \varphi_L C_T, \tag{12}$$

where the concentration in blood vessels can be expressed as

$$C_{\mathrm{pT}} = C_{0\mathrm{T}} \exp(-t/k_{\mathrm{dT}}).$$

Variables σ_{T}, $C_{0\mathrm{T}}$, k_{dT} indicate the osmotic reflectance coefficient of TSL, the initial concentration of TSL injection, and the decay time constant of TSL in the blood, respectively.

TSL will release the therapeutic drug DOX under the actual heating conditions, which then diffuses freely in the tumor cell stroma with a free drug concentration as[27]

$$\frac{\partial C_{\mathrm{F}}}{\partial t} = D_{\mathrm{F}}\nabla^2 C_{\mathrm{F}} - \boldsymbol{v}_{\mathrm{i}} \cdot \nabla C_{\mathrm{F}} - \frac{1}{\chi} K_{\mathrm{ON}} C_{\mathrm{rec}} C_{\mathrm{F}} + K_{\mathrm{EL}} C_{\mathrm{T}} + K_{\mathrm{OFF}} C_{\mathrm{B}}, \tag{13}$$

where drug-related parameters C_{F}, D_{F}, χ, K_{ON}, C_{rec}, K_{OFF} indicate free concentration, diffusion coefficient, accessible tumor volume fraction, binding rate, concentration at cell surface receptors, and dissociation rate, respectively.

Free drugs will bind to specific receptors on their surface after reaching malignant tissue during diffusion in the interstitium. The concentration of the binding drug can be described as[27]

$$\frac{\partial C_{\mathrm{B}}}{\partial t} = \frac{1}{\chi} K_{\mathrm{ON}} C_{\mathrm{rec}} C_{\mathrm{F}} - K_{\mathrm{OFF}} C_{\mathrm{B}} - K_{\mathrm{INT}} C_{\mathrm{B}}, \tag{14}$$

where K_{INT} represents the rate of drug internalization.

In fact, not all drugs bound to tumor tissue can exert therapeutic effects in tumor treatment, but only drugs that are successfully internalized by tumor cells and act on their internal mechanisms at the same time can effectively treat tumor cells. The internalized drug concentration can be expressed as[27]

$$\frac{\partial C_{\mathrm{I}}}{\partial t} = K_{\mathrm{INT}} C_{\mathrm{B}}. \tag{15}$$

The combination therapy proposed in this study can result in a dual effect of thermal and drug damage to tumor cells, and the degree of damage was closely related to both the therapeutic temperature distribution and the internalized drug concentration distribution. Thermal damage by magnetic hyperthermia should work in a specific temperature range between 42 °C and 46 °C, in which tumor cells can be effectively damaged, but not the healthy tissues.[28] According to a previous study, thermal damage can be expressed as[29]

$$\mathrm{FCK_h} = 1 - \exp\left(\int_0^t A\,\mathrm{e}^{-\Delta E/RT(t)}\,\mathrm{d}t\right), \tag{16}$$

where the related variables in Eq. (16) have their specific values given by a frequency factor of $A = 1.98 \times 10^{106}$ s^{-1}, an activation energy of $\Delta E = 6.67 \times 10^5$ J/mol, and the universal gas constant with value $R = 8.314$ J/(mol·K).

Drug damage is determined by the concentration of internalized drug with the following equation:[27]

$$\mathrm{FCK_i} = 1 - \exp\left(-w_{\mathrm{s}} \cdot C_{\mathrm{I}}\right), \tag{17}$$

where the survival constant of tumor cells, w_{s}, has the value 0.6603 m^3/mol.

3. Boundary conditions and materials properties

3.1. Boundary condition

All these equations presented above are calculated by the finite element method, which can just obtain a convergence result with proper setting of boundary conditions. Thus, this study has configured the appropriate boundary conditions for each model in order to ensure the reliability of the results obtained by solving the mathematical models. The pressure is set to 25 mmHg for the two inlets and to 10 mmHg for the outlet.[30] In addition, the boundary conditions of the blood vessel wall are set to a non-slip state. Initial values are set to zero for both IBP and IVP, and to 37 °C for therapeutic temperature. Both strategies of MNPs and TSL have the same initial concentrations, zero. The interface between tumor and healthy tissue should be continuous in the temperature, concentration, and interstitial pressure.[31]

3.2. Characteristics of the parameters

After constructing a physical field model with the required boundary condition constraints, the corresponding physical field can then be solved using the finite element method after combining precise parameters for the proposed model. Table 1 shows the parameters required to solve fluid pressure and flow velocity, in which the subscript is used to distinguish different biological tissues.

Table 1. Parameters for solving the pressure and velocity of blood and interstitial fluids.[27]

Parameter	Value	Unit
μ	0.004	Pa·s
K_0	2.5592×10^{-17}	m^2
K_1	1.2391×10^{-16}	m^2
$(L_{\mathrm{P}})_0$	0.36×10^{9}	m/((mmHg)·s)
$(L_{\mathrm{P}})_1$	2.8×10^{9}	m/((mmHg)·s)
$(L_{\mathrm{PL}}S_{\mathrm{L}}/V)_0$	1.33×10^{-5}	1/((mmHg)·s)
$(L_{\mathrm{PL}}S_{\mathrm{L}}/V)_1$	0	1/((mmHg)·s)
$(\sigma_{\mathrm{s}})_0$	0.91	–
$(\sigma_{\mathrm{s}})_1$	0.82	–
π_{b}	20	mmHg
$(\pi_{\mathrm{i}})_0$	10	mmHg
$(\pi_{\mathrm{i}})_1$	15	mmHg
$(S/V)_0$	700	1/m
$(S/V)_1$	20000	1/m
P_{L}	0	Pa

Table 2 shows the MNP-related parameters, which are used to solve the concentration of MNPs and the relevant parameters of heat transfer model in this study.

Table 2. MNP-related parameters.[20]

Parameter	Value	Unit
K_B	1.38×10^{-23}	J/K
a_N	6	nm
a_f	200	nm
η	1.38×10^{-4}	Pa·s
γ	0.66	–
σ_N	0.15	–
λ_0	3.75×10^{-7}	m/s
λ_1	3×10^{-6}	m/s
β	7.32×10^{-4}	1/s
f	300	kHz
H_m	24	kA/m
M_d	446	kA/m
k_{dN}	5193	s

Table 3 shows the material properties for each biological tissue, which are used to solve the biological heat transfer model.

Table 3. Characteristics of various biological tissue materials.[32]

Parameter	Liver tissue	Tumor	Blood	MNPs	Unit
ρ	1064	1060	1050	5180	kg/m^3
k	0.59	0.52	0.52	40	W/(m·K)
c	4180	3540	4180	4000	J/(kg·K)
Q_m	5790	684	–	–	W/m^3

Due to the movement of MNPs in the tumor stroma, the material properties of MNPs are influenced by both the tumor characteristics and MNP characteristics prior to injection:[32]

$$\begin{aligned}\rho &= \theta\rho_{MNP}+(1-\theta)\rho_{tumor},\\ c &= \theta c_{MNP}+(1-\theta)c_{tumor},\\ 1/k &= \theta/k_{MNP}+(1-\theta)/k_{tumor},\end{aligned}\tag{18}$$

where the volume fraction of MNPs, θ, can further be expressed as: $\theta = C_i/\rho_{MNP}$. Table 4 describes the characteristics of TSL and its released DOX in the drug delivery equation.

Table 4. Parameters related to TSL and DOX.[27]

Parameter	Value	Unit
D_T	7×10^{-12}	m^2/s
$(D_F)_0$	1.58×10^{-10}	m^2/s
$(D_F)_1$	3.4×10^{-10}	m^2/s
χ	0.4	–
K_{ON}	15	m^3/(mol·s)
C_{rec}	1×10^{-5}	M
K_{OFF}	8×10^{-3}	1/s
K_{INT}	5×10^{-5}	1/s
k_{dT}	1320	min

In addition, the variable K_{EL} should normally be significantly affected by temperature change in the TSL concentration model, and its corresponding relationship is listed in Table 5. As can be seen, the TSL does not have the ability to release drugs below the temperature of 37 °C, but begins to show an increasing trend with the gradual increase in temperature. When the temperature exceeds 42 °C, the K_{EL} value tends to settle and no longer changes with the increase in temperature. Notably, the release rate between temperature points can be predicted by the linear interpolation method.

Table 5. TSL release rate at different temperatures.[33]

T (°C)	37	38	39	40	41	42
K_{EL} (s^{-1})	0.004	0.005	0.015	0.028	0.043	0.054

4. Results and discussion

In the calculation process, the determined model parameters are input into the corresponding physical field models, which are then solved in the predetermined order. In this process, the blood pressure inside blood vessels is coupled with the interstitial fluid pressure, which can thereby obtain the interstitial fluid velocity. At the same time, the interstitial fluid velocity is further coupled with the concentrations of MNPs and TSL, and the temperature field also forms a coupling effect with the TSL concentration field. Figure 3 clearly illustrates these coupling relationships and the solution process, which can ensure the comprehensiveness and accuracy of the simulation results.

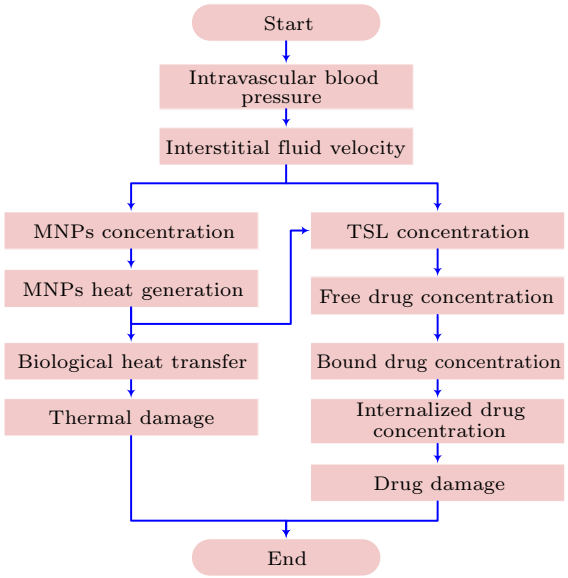


Fig. 3. Simulation flowchart for combination therapy.

4.1. Blood pressure and velocity distribution within blood vessels

Based on the calculation process in Fig. 3, intravascular blood pressure can be obtained by solving the related partial

differential model presented in Subsection 2.2. Figure 4 illustrates the distribution of blood pressure and flow velocity within blood vessels. As shown in Fig. 4(a), the significant characteristic for blood pressure distribution is that it reaches the maximum value of 3340 Pa in the adjacent areas of the two inlets of the blood vessel. Furthermore, the pressure of blood vessels shows a decreasing trend with the blood flow, that is, the pressure gradually decreases from the two inlet points towards the outlet. Finally, the pressure decreases to a minimum of 1630 Pa at the outlet of the blood vessel. In addition, it can be understood from Fig. 4(b) that the intravascular blood velocity can reach its maximum value of 17×10^{-2} m/s at the outlet of the blood vessel.

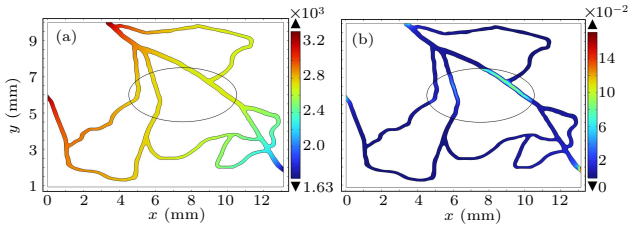


Fig. 4. Different physical field distribution for intravascular blood. (a) pressure; (b) flow velocity.

4.2. Pressure and velocity distribution for interstitial fluid

The Starling equation describes the coupling relationship between IBP and IFP, which also indicates that the intravascular blood pressure will affect the distribution of interstitial fluid pressure. According to Fig. 5(a), the pressure of interstitial fluid in tumor is significantly higher than that of healthy tissue due to the absence of an effective tumor lymphatic system. In Fig. 4(a), it is worth noting that the left vascular pressure inside tumor is higher than the right vascular pressure, which thereby leads to a higher interstitial fluid pressure on the left side of the tumor than on the right side. This phenomenon underscores the interaction and influence between endovascular blood pressure and interstitial hydraulics. This pressure difference promotes the maximum velocity of the interstitial fluid at the interface between tumor stroma and healthy tissue, as shown in Fig. 5(b). The direction of fluid flow is presented by the red arrow in Fig. 5(b), which also means that the direction of the flow towards the healthy tissue can actually hinder the diffusion of nanoparticles toward the tumor center.

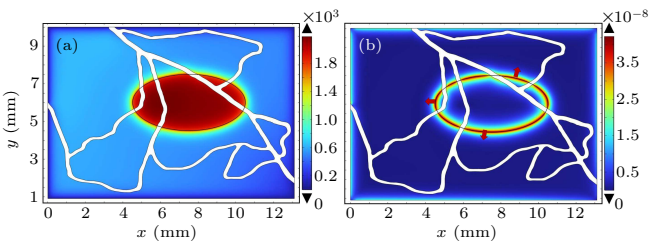


Fig. 5. Different physical field distributions for the interstitial fluid: (a) pressure, (b) flow velocity.

4.3. Distribution of MNP concentration under different injection strategies

The velocity field of the interstitial fluid provides convective velocity for the motion of MNPs. MNPs are directed into the human body through intravenous injection and then penetrate the wall of the blood vessel into the body. However, MNPs can only penetrate into the interstitial region of the tumor due to the limitation of the pore size of the vascular wall in healthy tissues.[34] In addition, this study proposes a delayed injection strategy for combination therapy in order to increase the therapeutic outcome, which infuses the TSL one hour after injecting MNPs, and then begins to heat the MNPs after two hours of particle diffusion. Instead, the direct injection strategy infuses the TSL after a two-hour interval of MNP injection, and then induces MNPs to produce heat under an external magnetic field.

Figure 6 shows the concentration profile of MNPs under different injection strategies before the magnetic field works. As depicted in Fig. 6, the area near blood vessels shows a higher profile of MNPs within the malignant stroma, in which the maximum concentration of MNPs is located in the area between two blood vessels. From the comparison of Figs. 6(a) and 6(b), the MNP concentration in the direct injection strategy is higher than in the delayed injection strategy due to its shorter decay time of MNPs in the blood. However, the shorter diffusion time of MNPs under the direct injection case also resulted in a more concentrated distribution of MNPs. As can be seen, the movement and distribution of MNPs in a living organism are significantly influenced by the velocity field of interstitial fluid due to its convective behavior. Although both strategies can result in a higher concentration distribution near blood vessels due to the MNPs penetration behavior from blood vessel walls to tumor stroma, the direct injection can have a higher and more concentrated situation due to its relatively shorter decay time with respect to the delayed injection.

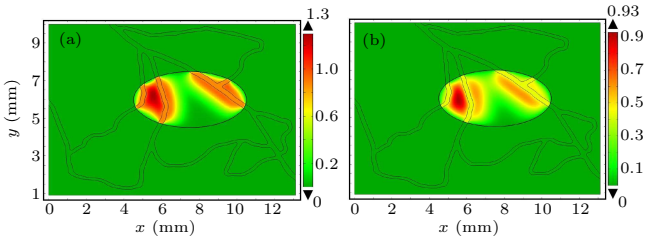


Fig. 6. Distribution of MNP concentration under different injection strategies: (a) direct injection, (b) delayed injection.

4.4. Therapeutic temperature distribution under different injection strategies

MNPs generate heat for both hyperthermia and drug release under the effect of a magnetic field, and this further elevates the local temperature for therapy. Figure 7 depicts the temperature field distribution of local temperature after 30 minutes of heat generation under different injection strategies. Particularly, when the direct injection strategy was con-

sidered in the study, the highest temperature can reach 46 °C due to its relatively clustered MNPs in a particular location. On the other hand, although the maximum value in the delayed injection case is only 43.2 °C, the temperature presents a more uniform distribution due to its more dispersed distribution of MNPs. Nevertheless, the result presented in Fig. 7(b) can actually be further improved by increasing the power dissipation of MNPs to a proposed value, in which the maximum temperature can also reach a critical safety value for therapy, which is 46 °C. As illustrated in Fig. 7(c), the whole temperature distribution can be improved effectively after considering this optimization method. In the process of delayed injection strategy with optimization, the delayed injection strategy promotes the diffusion of MNPs to tumor region and also increases the required MNPs power dissipation for critical temperature, which can then be effectively improved and perfected by the improvement of MNPs power dissipation due to magnetic field intensity. Thus, both uniformity and amplitude of temperature distribution in Fig. 7(c) can receive an overall increase with respect to other two cases presented in Figs. 7(a) and 7(b).

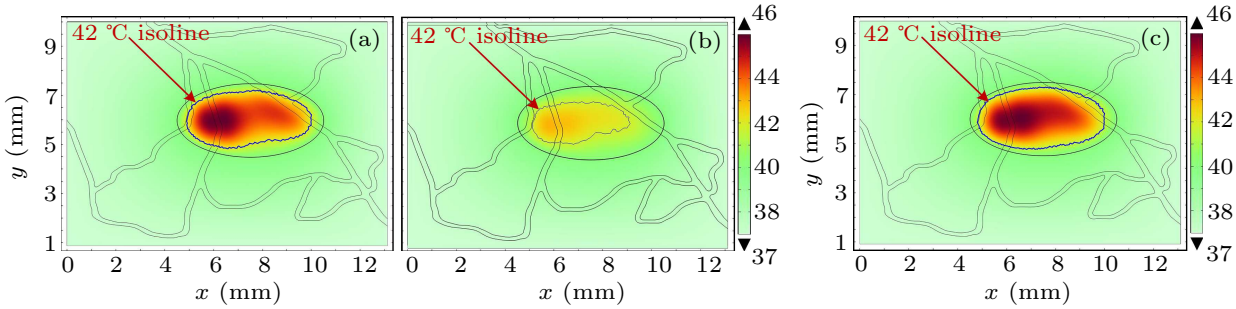


Fig. 7. Temperature profile under different injection strategies: (a) direct injection, (b) delayed injection, (c) delayed injection after improvement.

In the proposed delay strategy with optimization, the delayed injection strategy can effectively widen the distribution range of MNPs, and the optimization method helps to improve the overall temperature distribution. The improvement in the results can be assessed using an evaluation index for the temperature distribution that is the effective area percentage of tumor temperature between 42 °C and 46 °C (EAPTT). As can be seen in Fig. 8, the EAPTT value drops from 66% to 38% after considering the delayed injection strategy, and then increases significantly to 74% when the optimization method is taken into consideration. Thus, this study will focus on the direct injection and the delayed strategy with optimization in the following section.

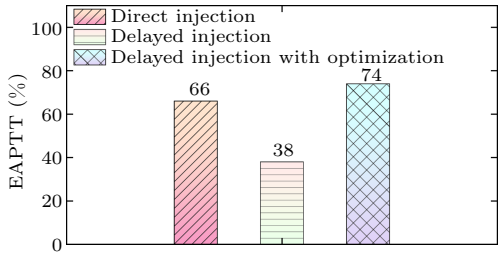


Fig. 8. EAPTT value for three different injection strategies.

4.5. Drug concentration distribution under different injection strategies

TSL will begin to release the drug DOX with the increase of tissue temperature due to the MNPs. Figure 9(a) shows the distribution of TSL concentration at the end of MNP thermogenesis under the direct injection strategy using a combination therapy. It can be observed that the TSL is concentrated mainly near the blood vessels, which can be attributed to the relatively short diffusion time of TSL, 30 min, in the direct injection strategy. Furthermore, the higher temperature near the blood vessel results in the release of TSL due to thermal triggering and in the aggregation of internalized drug near the blood vessel, as illustrated in Fig. 9(b).

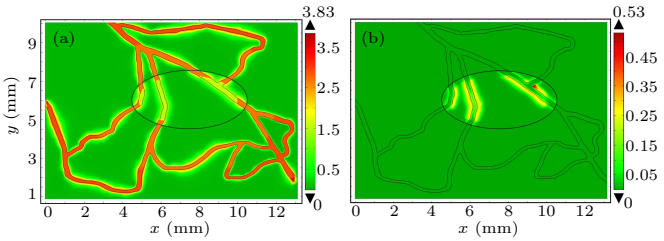


Fig. 9. Drug concentration distribution under direct injection strategy: (a) TSL concentration, (b) internalized drug concentration.

Figure 10(a) shows the distribution of TSL concentration after 2 hours of diffusion under the delayed injection with optimization in the combination therapy. TSL penetrates into the tumor region by the blood vessel, so the TSL concentration has a maximum value near the blood vessel and gradually decreases away from it. As MNPs generate heat, the TSL appears to have the fastest release rate in the middle area of the two leftmost blood vessels due to its maximum temperature, as described in Fig. 10(b).

It can also be understood that the decrease in the TSL concentration is most significant in this region. Accordingly, the concentration of the internalized drug reached its maximum

value around the two blood vessels, and both its concentration value and distribution range are better than those under the direct injection strategy, as depicted in Fig. 10(c). This phenomenon can be explained as the fact that when the temperature exceeds a specific release threshold of the TSL, 42 °C, the drug DOX begins to release due to the reduced stability of the TSL's bilayer membrane. In comparison with the direct injection, the optimized delayed injection strategy achieves a wider and more uniform drug distribution by adjusting the injection and diffusion time for MNPs, since the sufficient diffusion time for TSL makes it no longer limited to the surrounding blood vessels but a wider area.

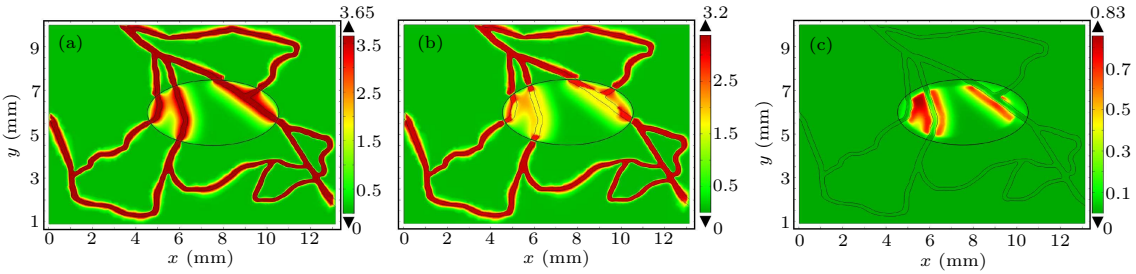


Fig. 10. Drug concentration under delayed injection strategy: (a) TSL concentration after diffusion, (b) TSL concentration at the end of MNP heat generation, (c) internalized drug concentration at the end of MNP thermogenesis.

4.6. Tumor damage distribution under different injection strategies

Once the combination therapy has been completed, the effectiveness of different injection strategies for combination therapy can be evaluated by the degree of tumor cell damage using Eqs. (16) and (17). The tumor damage consists of two indexes, thermal damage due to MNPs and drug damage due to DOX. Figure 11 describes the thermal damage distribution for two different injection strategies. It can be easily understood that this thermal damage situation is positively correlated with the therapeutic temperature distribution during this combination therapy. Specifically, the maximum temperature under both injection strategies is the same, which results in the same outcome in the maximum thermal damage. However, the delayed injection strategy with optimization has an obvious advantage in the distribution of thermal damage along the tumor region.

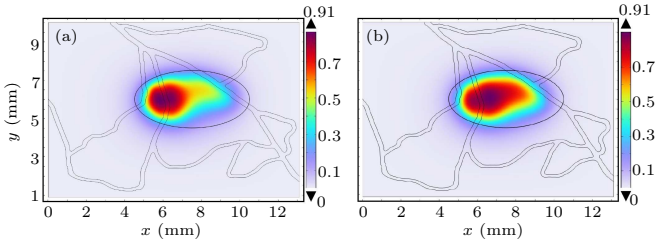


Fig. 11. Thermal damage under different injection strategies: (a) direct injection, (b) delayed injection.

In addition, the DOX released by TSL can result in the drug damage, and its degree of damage has a direct correlation with the concentration of internalized drug inside the tumor region. Figure 12 depicts the drug damage to tumor cells under different injection strategies during therapy. As can be seen in Fig. 12(a), a significant value of the degree of drug damage can only be observed in the relatively limited vicinity of blood vessels in the direct injection strategy, so the treatment effect is relatively low. In contrast, this poor situation of drug damage in the direct injection strategy can be greatly improved in both the maximum extent and the scope under the delayed injection strategy, as shown in Fig. 12(b). It can be observed that the optimized delayed injection strategy exhibits a more uniform distribution in the thermal and drug damage, which also reflects its good therapeutic effect with respect to the direct injection. This phenomenon can be mainly attributed to the high uniform distribution of MNPs and drug DOX within the tumor area under this delayed injection strategy. In addition, the distribution of damage model reveals that thermal and drug damage are consistent with the concentration of temperature and internalized drug, respectively.

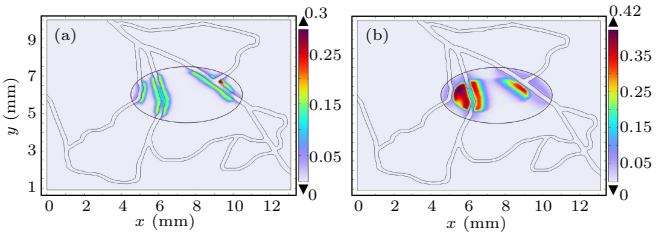


Fig. 12. Drug damage under different injection strategies: (a) direct injection, (b) delayed injection.

In order to validate the reliability and accuracy, the results by this study also are compared with previous literature in the aspect of IFP, IFV, the local temperature, and also the treatment effect. Compared with the result by previous report,[35] both the IFP and IFV in this study have the similar change trend, but the IFP presents a higher amplitude due to the consideration of blood pressure, as shown in Fig. 13(a). In addition, both injection strategies in this study have the similar trend of maximum temperature with Liu *et al.*,[36] and have a little better than Stylianopoulos *et al.* in FCK value.[37] Thus, it can be concluded that this study is basically consistent with previous research findings.

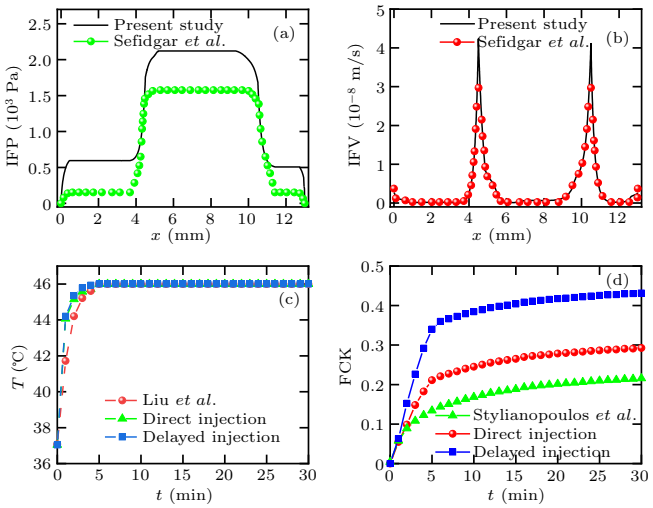


Fig. 13. Result comparisons of different parameters between present study and previous reports: (a) IFP, (b) IFV, (c) treatment temperature, (d) FCK.

5. Conclusion

This study innovatively proposes the direct and delayed injection strategies based on the synchronous intravenous injection method of MNPs and TSL, and further effectively improves the combination therapy by regulating the MNPs power dissipation accurately for the improved delayed strategy. In addition, a relatively complex geometric model is used for the theoretical verification, in which the effect of blood pressure on both the pressure and velocity of interstitial fluid are also taken into consideration for this study. Simulation results demonstrate that the MNP concentration in the direct injection case is higher than that in the delayed injection due to the shorter decay time of MNPs in the blood, and this situation can then result in a larger effective temperature area and further improve the degree of thermal damage to tumor cells. However, the TSL in the direct strategy can release the DOX directly by heat, which leads to a lower concentration of internalized drug and a limited degree of drug damage. In addition, the results also reveal that the proposed delayed injection strategy after optimization can effectively overcome the general shortage of lower temperature in the treatment area and also allow the TSL enough time to diffuse within the tumor stroma and to improve drug damage due to the increase in the concentration of internalized drug. In summary, the proposed delayed injection strategy after optimization can present an excellent therapeutic effect on the combination therapy of magnetic hyperthermia and thermosensitive liposomes, which can provide the scientific basis and practical direction for the development of future combination therapy strategies.

Acknowledgements

Project supported in part by the National Natural Science Foundation of China (Grant Nos. 62471144 and 62071124) and in part by the Conselho Nacional de Desenvolvimento Científico e Tecnológico (BR) (CNPq) (Grant No. 315546/2021-2).

References

[1] Darwish M S, Al-Harbi L and Bakry A 2022 *J. Therm. Anal. Calorim.* **147** 11921
[2] Li W Y, Li W T, Li B Q, Dong L J, Meng T H, Huo G, Liang G Y and Lu X G 2021 *Chin. Phys. B* **30** 104402
[3] Włodarczyk A, Gorgoń S, Radoń A and Bajdak-Rusinek K 2022 *Nanomaterials* **12** 1807
[4] Regenold M, Bannigan P, Evans J C, Waspe A, Temple M J and Allen C 2022 *Nanomedicine: Nanotechnol., Biol. Med.* **40** 102484
[5] Motamarry A, Wolfe A M, Ramajayam K K, Pattanaik S, Benton T, Peterson Y, Faridi P, Prakash P, Twombley K and Haemmerich D 2022 *Cancers* **14** 1322
[6] Kashkooli F M, Soltani M and Souri M 2020 *J. Control. Release* **327** 316
[7] Amin M, Seynhaeve A L, Sharifi M, Falahati M and Ten Hagen T L 2022 *Pharmaceutics* **14** 2165
[8] Rezaeian M, Sedaghatkish A and Soltani M 2019 *Drug Deliv.* **26** 898
[9] Fortes Brollo M E, Dominguez-Bajo A, Tabero A, Dominguez-Arca V, Gisbert V, Prieto G, Johansson C, Garcia R, Villanueva A and Serrano M C 2020 *ACS Appl. Mater. Interfaces* **12** 4295
[10] Tehrani M H, Soltani M, Moradi Kashkooli F, Mahmoudi M and Raahemifar K 2021 *Pharmaceutics* **14** 35
[11] Hernandez J L and Woodrow K A 2022 *Adv. Healthcare Mater.* **11** 2102087
[12] Wang G, Wu B, Li Q, Chen S, Jin X, Liu Y, Zhou Z, Shen Y and Huang P 2020 *Small* **16** 2004172
[13] Chen J, Wang C and Mo R 2023 *Chin. Phys. B* **32** 094302
[14] Suleman M and Riaz S 2020 *Med. Eng. Phys.* **86** 128
[15] Soltani M and Chen P 2011 *PloS One* **6** e20344
[16] Kim S and Kim M C 2002 *Int. Commun. Heat Mass Transfer* **29** 127
[17] Starling E H 1896 *J. Physiol.* **19** 312
[18] Moghadam M C, Deyranlou A, Sharifi A and Niazmand H 2015 *Microvasc. Res.* **101** 62
[19] Li R N, Da X H, Li X, Lu Y S, Gu F F and Liu Y 2021 *Chin. Phys. B* **30** 017502
[20] Shojaee P, Niroomand-Oscuii H, Sefidgar M and Alinezhad L 2020 *J. Magn. Magn. Mater.* **498** 166089
[21] Shamsi M, Sedaghatkish A, Dejam M, Saghafian M, Mohammadi M and Sanati-Nezhad A 2018 *Drug Deliv.* **25** 846
[22] Dewhirst M W and Secomb T W 2017 *Nat. Rev. Cancer* **17** 738
[23] Tang Y, Zou J, Flesch R C, Jin T and He M H 2022 *Chin. Phys. B* **31** 014401
[24] Tang Y, Chen M, Flesch R C and Jin T 2023 *Chin. Phys. B* **32** 094401
[25] LeBrun A, Ma R and Zhu L 2016 *J. Therm. Biol.* **62** 129
[26] Namakshenas P and Mojra A 2023 *Int. J. Mech. Sci.* **237** 107818
[27] Moradi Kashkooli F, Soltani M, Momeni M M and Rahmim A 2021 *Front. Oncol.* **11** 655781
[28] Tang Y, Zou J, Flesch R C and Jin T 2023 *Chin. Phys. B* **32** 034304
[29] Gasselhuber A, Dreher M R, Negussie A, Wood B J, Rattay F and Haemmerich D 2010 *Int. J. Hyperthermia* **26** 499
[30] McDougall S R, Anderson A R A and Chaplain M A J 2006 *J. Theor. Biol.* **241** 564
[31] Javidi M, Heydari M, Karimi A, Haghpanahi M, Navidbakhsh M and Razmkon A 2014 *J. Biomed. Phys. Eng.* **4** 151 PubMed PMID: 25599061; PubMed Central PMCID: PMC4289522
[32] Tang Y, Wang Y, Flesch R C and Jin T 2023 *J. Phys. D: Appl. Phys.* **56** 145402
[33] Moradi Kashkooli F, Souri M, Tavakkoli J and Kolios C M 2023 *Drug Deliv.* **30** 2219871
[34] Ramajayam K K, Newton D A and Haemmerich D 2022 *Int. J. Hyperthermia* **39** 998
[35] Sefidgar M, Bashooki E and Shojaee P 2020 *J. Therm. Biol.* **94** 102742
[36] Liu K C and Chen T M 2021 *J. Therm. Biol.* **98** 102907
[37] Stylianopoulos T, Economides E A, Baish J W, Fukumura D and Jain R K 2015 *Ann. Biomed. Eng.* **43** 2291